π kinks in a parametrically driven sine-Gordon chain

Yuri S. Kivshar*
Departamento de Fisica Teorica I, Facultad de Ciencias Fisicas, Universidad Complutence, 28040 Madrid, Spain

Niels Grønbech-Jensen
Department of Applied Physics, Stanford University, Stanford, California 94305

Mogens R. Samuelsen
Physics Laboratory I, The Technical University of Denmark, 2800 Lyngby, Denmark
(Received 16 August 1991)

We consider the sine-Gordon chain driven by a high-frequency parametric force in the presence of loss. Using an analytical approach based on the method of averaging in fast oscillations, we predict that such a parametric force may support propagation of π kinks, which are unstable in the standard sine-Gordon model. The steady-state velocity of the π kinks is calculated, and the analytical results are in good agreement with direct numerical simulations.

I. INTRODUCTION

The sine-Gordon (SG) system is known to model many physical objects in the framework of one-dimensional approximations such as flux motion in Josephson junctions, dislocations in solids, nonlinear spin waves in the superfluid phases of ^{3}He, ferromagnetic and antiferromagnetic systems, etc. (see some references, e.g., in the review paper Ref. 1). The simplest localized solutions of the system are the so-called kinks which describe motion of topological excitations, for example, fluxons in long Josephson transmission lines or various domain walls in magnetic systems. The kink connects two nearest ground states of the system, e.g., $u=0$ and $u=2\pi$, u being the angle variable, so that it may be called a 2π kink. In real physical systems when dissipative losses are included, kinks may exist in the form of state configurations, and they move under an external constant force.[1] In a number of physically important systems, an applied force is periodic in time. Detailed investigations of the ac driven SG system with loss show a lot of interesting features of the system dynamics, e.g., spatial-temporal complexity and chaos (see, e.g., Refs. 2 and 3). In some physical systems, e.g., magnetic chains, the applied periodic force acts as a parametric force (see, e.g., Refs. 4–6 and references therein). As is well known,[4] a low-frequency (LF) parametric force may stabilize the breather when the frequency of the external force lies in the gap of the linear spectrum. However, such a LF parametric force has no strong influence on the kink dynamics.[1] It is the purpose of this paper to analyze the influence of a high-frequency (HF) parametric force on the SG system dynamics. Using an analytical approach and direct numerical simulations, we demonstrate that the parametrically driven SG system may support propagation of the π kinks (which are unstable in the standard SG model) when the frequency of the force is large enough. Due to the existence of these π kinks, the shape of the 2π kinks may be more complicated and it is described by an effective double-SG equation. We also study the dynamics of the envelope solitons excited at $u=\pi$ which are stable under the influence of the HF parametric force only.

II. ANALYTICAL APPROACH

A. General formalism

Let us consider a discrete nonlinear chain under the influence of a parametric force and in the presence of dissipative loss. The model equation is

$$\ddot{\phi}_n - K(\phi_{n-1} - 2\phi_n + \phi_{n+1}) + \frac{dV(\phi_n)}{d\phi_n} = A\cos(\omega t)G(\phi_n) - \gamma\dot{\phi}_n , \quad (1)$$

where A and ω are the normalized amplitude and frequency of the periodic force, respectively, and γ is the normalized dissipative coefficient. The parameter K describes a coupling between particles in the chain, $V(\phi)$ is the normalized external potential and the function $G(\phi)$ characterizes the parametric force. For the parametrically driven SG model which is considered in this paper we take

$$V(\phi)=1-\cos(\phi) , \quad (2)$$

$$G(\phi)=\sin(\phi) . \quad (3)$$

Without a perturbation, Eqs. (1) and (2) describe the well-known SG model, i.e., a chain of interacting particles in the harmonic periodic potential. In the continuum limit, when $\phi_{n\pm1}\approx\phi_n\pm a\phi_n'+\frac{1}{2}a^2\phi_n''$, the SG system supports the kink solution,

$$\phi(x,t)=\pm 4\tan^{-1}\exp\left[\frac{x-vt}{\sqrt{c^2-v^2}}\right] , \quad (4)$$

where a is the normalized lattice spacing, t is a normalized time, v is the normalized kink velocity, and

$c=a\sqrt{K}$ is the normalized limit velocity. Small amplitude excitations of the discrete chain near the minima of the potential are linear waves with the dispersion law,

$$\Omega^2=1+4K\sin^2\left[\frac{qa}{2}\right], \tag{5}$$

i.e., the system eigenfrequencies lie in the region $\Omega^2_{\min}<\Omega^2<\Omega^2_{\max}$, where $\Omega^2_{\min}=1$ and $\Omega^2_{\max}=1+4K$.

We will consider the perturbed system Eq. (1) assuming that the frequency ω is large enough to be outside of the region of parametric instability of linear waves. To describe the nonlinear dynamics under influence of such a HF parametric force, we will use the method of averaging which is analogous to that for the well-known Kapitza problem, i.e., dynamics of a pendulum with an oscillating pivot (see Ref. 7). To derive an averaged equation of motion for the system dynamics, we will consider the wave field ϕ_n as a sum of slowly and fast varying parts, i.e.,

$$\phi_n(t)=\Phi_n(t)+\xi_n(t), \tag{6}$$

where the function $\xi_n(t)$ describes the fast oscillations ($|\dot{\xi}_n|\gg|\xi_n|$). Substituting Eq. (6) into Eq. (1), and using the expansion in the small ξ_n, we obtain the equation

$$\ddot{\Phi}_n+\ddot{\xi}_n-K(\Phi_{n-1}-2\Phi_n+\Phi_{n+1})-K(\xi_{n-1}-2\xi_n+\xi_{n+1})+V'(\Phi_n)+\xi_n V''(\Phi_n)+\tfrac{1}{2}\xi_n^2 V'''(\Phi_n)$$
$$=A\cos(\omega t)G(\Phi_n)+A\cos(\omega t)\xi_n G'(\Phi_n)-\gamma\dot{\Phi}_n-\gamma\dot{\xi}_n . \tag{7}$$

If the force frequency lies outside of the region of the parametric resonance, $\Omega^2_{\min}<(\Omega/2)^2<\Omega^2_{\max}$, the periodic force cannot excite waves in the system. Hence, it is reasonable to assume that the function $\xi_n(t)$ does not depend on n, i.e., $\xi_{n\pm1}\approx\xi_n$. It is clear that Eq. (7) has terms of different nature, slowly and fast varying. These different terms have to be compensated separately. It means that for fast oscillations the following equation has to be valid,

$$\ddot{\xi}_n+\xi_n V''(\Phi_n)=A\cos(\omega t)G(\Phi_n)-\gamma\dot{\xi}_n , \tag{8}$$

and in Eq. (8) the function $G(\Phi)$ may be considered as a constant value. As a result, the forced solution of Eq. (8) has the form

$$\xi_n(t)=\frac{AG(\Phi_n)}{\sqrt{(\omega^2-\omega_0^2)^2+\gamma^2\omega^2}}\cos(\omega t+\delta) , \tag{9}$$

where

$$\cos\delta=-\frac{(\omega^2-\omega_0^2)}{\sqrt{(\omega^2-\omega_0^2)+\gamma^2\omega^2}} \tag{10}$$

and

$$\omega_0^2\equiv V''(\Phi_n) . \tag{11}$$

Substituting Eqs. (9) and (10) into Eq. (7) and averaging in fast oscillations, we may obtain the equation for the slowly varying function $\Phi_n(t)$,

$$\ddot{\Phi}_n+\gamma\dot{\Phi}_n-K(\Phi_{n-1}-2\Phi_n+\Phi_{n+1})+V'(\Phi_n)$$
$$=-\frac{A^2G^2(\Phi_n)V'''(\Phi_n)}{4[(\omega^2-\omega_0^2)^2+\gamma^2\omega^2]}$$
$$-\frac{A^2(\omega^2-\omega_0^2)G'(\Phi_n)G(\Phi_n)}{2[(\omega^2-\omega_0^2)^2+\gamma^2\omega^2]} , \tag{12}$$

where ω_0^2 is defined by Eq. (11). To obtain the RHS of Eq. (12), we have used the following results:

$$\langle\xi_n V''(\phi_n)\rangle=0 ,$$
$$\langle\xi_n^2\rangle=\frac{1}{2}\frac{A^2G^2(\Phi_n)}{2(\omega^2-\omega_0^2)^2+\gamma^2\omega^2} ,$$

and

$$\langle a\cos(\omega t)\xi_n(t)\rangle=\frac{A^2G(\Phi_n)\cos\delta}{2\sqrt{(\omega^2-\omega_0^2)^2+\gamma^2\omega^2}}$$
$$=-\frac{A^2G(\Phi_n)(\omega^2-\omega_0^2)}{2[(\omega^2-\omega_0^2)^2+\gamma\omega^2]} ,$$

where the brackets stand for the averaging in fast oscillations with frequency ω. In the case $\omega^2\gg\omega_0^2$, i.e., in fact in the region $\omega^2>\Omega^2_{\max}$ (to be outside of the region of parametric resonance), the first term in the RHS of Eq. (12) may be omitted because it is much smaller than the second one, and Eq. (12) takes the form

$$\ddot{\Phi}_n-K(\Phi_{n-1}-2\Phi_n+\Phi_{n+1})+\frac{dV_{\text{eff}}}{d\Phi_n}=-\gamma\dot{\Phi}_n , \tag{13}$$

where

$$V_{\text{eff}}(\Phi)=V(\Phi)+\frac{A^2G^2(\Phi)}{4(\omega^2+\gamma^2)} . \tag{14}$$

Equations (13) and (14) describe averaging dynamics of the parametrically driven SG system with loss.

B. π kinks

For the SG model defined in Eqs. (1)–(3), the effective potential of Eq. (14) may be written as

$$V_{\text{eff}}(\Phi)=1-\cos\Phi+\frac{A^2\sin^2\Phi}{4(\omega^2+\gamma^2)} , \tag{15}$$

and the equation of motion (13) takes the form of the discrete double-SG (DSG) equation

$$\ddot{\Phi}_n - K(\Phi_{n-1} - 2\Phi_n + \Phi_{n+1}) + \sin\Phi_n + \frac{A^2}{4(\omega^2+\gamma^2)}\sin(2\Phi_n) = -\gamma\dot{\Phi}_n \ . \quad (16)$$

The effective potential energy Eq. (15) has two different states when the parameter A is changing. If

$$A^2 > A_{cr}^2 = 2(\omega^2+\gamma^2) \ , \quad (17)$$

the potential of Eq. (15) has additional minima at $\Phi = \pi + 2\pi n$ ($n = 0, \pm 1, \ldots$) (see Fig. 1). In the continuum limit, i.e., when the expression $\phi_{n\pm1} \approx \phi_n \pm a\phi_n' \pm \frac{1}{2}a^2\phi_n''$ is valid, Eq. (16) has the static solution in the form of the 2π kink.[8] However, when $A^2 > A_{cr}^2$, the effective potential Eq. (15) supports also stable propagation of the π kink,

$$\Phi(x,t) = 2\tan^{-1}\left[\exp\left[\frac{A(x-V_* t)}{A_{cr}\sqrt{c^2-V_*^2}}\right]\right] , \quad (18)$$

where V_* is the normalized steady-state velocity of the π kink. This solution is unstable in the standard SG model. Unlike the 2π kink,[8] the solution Eq. (18) has a nonzero velocity which is determined by the amplitude of the driving force and dissipation,

$$V_* = \frac{c}{\left[1+\frac{A^2\gamma^2}{2(\omega^2+\gamma^2)}\right]^{1/2}} \ . \quad (19)$$

Here, we must, of course, require that the condition of Eq. (17) is fulfilled. The π kink Eqs. (18) and (19) is an exact solution of Eq. (16) in the continuum approximation. In fact, it may be obtained from the steady-state kink solution of the perturbed SG equation

$$u_{tt} - u_{xx} + \sin u = 2h\sin(u/2) - \gamma u_t \ , \quad (20)$$

which was analyzed in Ref. 9. Due to difference between the energy values at $\Phi = 0$ and $\Phi = \pi$, such a solution cannot be static, and it moves at a fixed velocity defined by the balance between the energy difference $\Delta E = E(\Phi=\pi) - E(\Phi=0)$ and dissipative losses.

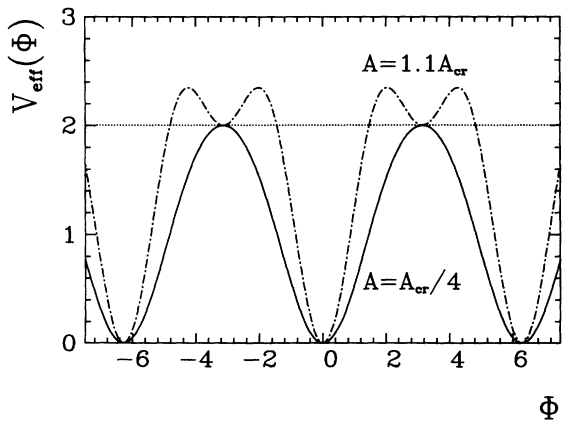

FIG. 1. The ac induced effective potential [Eq. (15)] as a function of the phase Φ for two different values of the driving amplitude. $A = 0.25 \cdot A_{cr}$ (solid) and $A = 1.10 \cdot A_{cr}$ (dashed).

C. Envelope solitons

As we can see from Eq. (15), the condition Eq. (17) means that the maximum of the potential V_{eff} at $\phi = \pi + 2\pi n$ is transformed into a minimum. Therefore, near the new minima of the potential it is possible to observe propagation of nonlinear excitations which are completely absent without a parametric driving force. To analyze such nonlinear excitations let us put $\Phi_n = \pi + \Psi_n$ and expand Eq. (16) at $\gamma = 0$ in Ψ_n,

$$\ddot{\Psi}_n - K(\Psi_{n-1} - 2\Psi_n + \Psi_{n+1}) + \Omega_0^2\Psi_n - \beta\Psi_n^3 = 0 \ , \quad (21)$$

where

$$\Omega_0^2 = \frac{A^2}{A_{cr}^2} - 1 \ , \qquad \beta = \frac{1}{6}\left[\frac{4A^2}{A_{cr}^2} - 1\right] \ . \quad (22)$$

We look for oscillating nonlinear solutions of Eq. (21) in the form

$$\Psi_n(t) = F_n(t)e^{i\Theta n} + \text{c.c.} \ , \quad (23)$$

where $\Theta_n = nqa - \Omega t$ is the phase of the wave in the discrete approximation, and the wave frequency Ω and wave number q are connected by the linear dispersion relation,

$$\Omega^2 = \Omega_0^2 + 4K\sin^2\left[\frac{qa}{2}\right] \ . \quad (24)$$

Such a discrete carrier approach allows us to use the discrete approximation for the carrier wave and the continuum approximation for the wave envelope $F_n(t)$. As a result the equation for the wave envelope has the form (see the similar calculations in Ref. 10),

$$iF_t + P(q)F_{zz} + Q|F|^2F = 0 \ , \quad (25)$$

$$z = x - V_g t, \quad V_g = \frac{\partial\Omega}{\partial q} = \frac{aK}{\Omega}\sin(qa) \ , \quad (26)$$

$$P(q) = \frac{Ka^2}{2\Omega}\left[\cos(qa) - \frac{K}{\Omega^2}\sin^2(qa)\right] \ , \quad (27)$$

$$Q = -\frac{3\beta}{2\Omega} \ . \quad (28)$$

Equation (25) is the well-known nonlinear Schrödinger equation and it has the soliton solution in the form,

$$F(z,t) = a\frac{\exp[\frac{1}{2}iVz - 4i(a^2 - \frac{1}{2}V^2)t]}{\cosh[a(z-Vt)]} \ . \quad (29)$$

Using the transformation to the initial variables, it is possible to obtain a localized solution of Eq. (21). It is important to note that such a localized soliton exists only at the condition $A^2 > A_{cr}^2$ when the square of the frequency Ω_0 defined by Eq. (22) is positive.

III. RESULTS OF NUMERICAL SIMULATIONS

We have considered a discrete system given by

$$\ddot{\phi}_n + \sin\phi_n - \frac{1}{\Delta x^2}(\phi_{n-1} - 2\phi_n + \phi_{n+1}) = -\gamma\dot{\phi}_n + A\sin\phi_n\cos(\omega t) , \quad (30)$$

where $i = 1,2,\ldots,1001$, and $\phi_0 = \phi_2$ and $\phi_{1002} = \phi_{1000}$ in order to simulate a long, but finite, size system. The total length of the system is given by the choice of $\Delta x = K^{-1/2} = 0.1$, which obviously results in a length of $L = 100$. In the simulations we have used a standard fourth-order Runge-Kutta method to integrate the system in time, but also a second-order explicit finite-difference method has been successfully tested and compared to the fourth-order Runge-Kutta method. The time step size was chosen to be $\Delta t = 0.01 \cdot 2\pi/\omega$ and this was found to be quite sufficient to describe the fast oscillating driving field.

The two conditions to be fulfilled by the parameters Δx, A, and ω are

$$\omega^2 > 4\left[1 + 4\frac{1}{\Delta x^2}\right] , \quad (31)$$

$$\omega^2 < \tfrac{1}{2}A^2 - \gamma^2 \simeq \tfrac{1}{2}A^2 . \quad (32)$$

By choosing $\Delta x = 0.1$ and $\omega = 100$ we find these to be

$$10^4 > 1604 , \quad (33)$$

$$A > \sqrt{2} \times 100 . \quad (34)$$

Clearly, the condition for not exciting the linear modes [Eqs. (31) and (33)] is fulfilled for these choices of parameters. In order to create an effective potential, we must choose A in accordance with Eq. (34). Also we must choose A so that the amplitude of the fast oscillating field (ξ) given by Eq. (9) fulfills the condition $|\xi_n(t)| \ll 1$. For the parameters chosen above, this is fulfilled for $A \ll \omega^2$.

Choosing the driving field amplitude $A = 250$ we have in fact observed stable and localized π kinks propagating through the system. Initially, we have placed a π kink with no velocity at the center of the system ($x = 50$). Typically in our simulations the speed of the kink, converting $\phi = \pi$ to $\pi = 0$, reached its steady-state velocity after approximately 10 normalized time units. In Fig. 2 we have shown the spatial section of the system between $x = 70$ and $x = 80$ as the kink passes through this region. In Fig. 2(a) the dissipation parameter γ has been chosen to $\gamma = 0$, whereas Fig. 2(b) shows the situation for $\gamma = 0.4$. What is interesting is here first of all to observe the localized π kink, but, secondly, also to observe the effect of the dissipation. In Fig. 2(a) we clearly observe a tail of radiative losses following the traveling kink. Since the traveling kink converts $\phi = \pi$ down to $\phi = 0$, the system will continuously experience a loss in potential energy, which must be converted into kinetic energy or dissipative loss. The radiation of energy is necessary contribution to the wave profile, in order to eliminate this excess energy in the steady-state motion. In the case of $\gamma = 0$ the decay of the radiated energy is ensured by the external parametric field if Eq. (31) is fulfilled. If we, on the other hand, supply the system with direct dissipation ($\gamma = 0.4$) as shown in Fig. 2(b), we find that this loss compensates the converted potential energy ($\phi = \pi \rightarrow \phi = 0$) so that no radiative losses are visible in the steady-state motion.

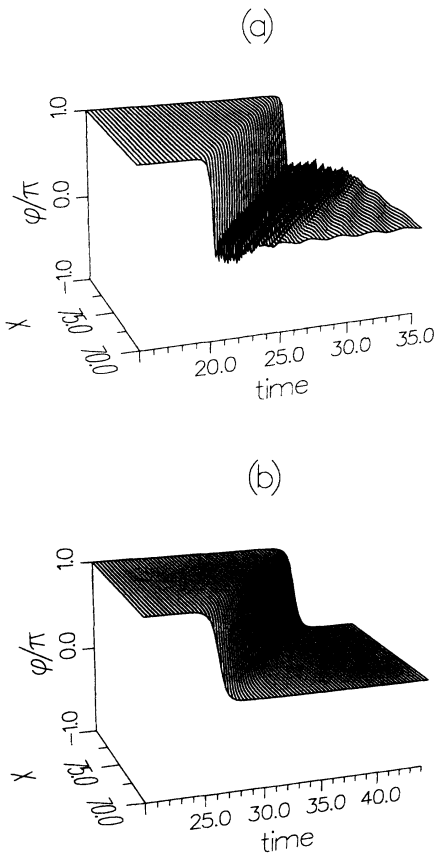

FIG. 2. Steady-state motion of a π kink. Parameters are $\Delta x = 0.1$, $L = 100$, $A = 250$, and $\omega = 100$. (a) $\gamma = 0$. (b) $\gamma = 0.4$.

In order to verify the power balance velocity of Eq. (19) of the traveling π kink in the parametrically driven system, we have performed numerical experiments for different driving amplitudes A and dissipation parameters γ, following the trace of the kink as a function of time. In Fig. 3 the results of the numerical experiments are shown. Here the perturbation prediction of the steady-state velocity is shown as curves of different types and the corresponding measurements of the π kink velocity made on the system Eq. (30) are shown as markers. The general behavior of the balance velocity is that the perturbation result seems to be a very good estimate for larger values of the dissipation parameter γ, where almost perfect agreement is found between the numerical experiments and the perturbation approach. However, for smaller γ the perturbation result estimates the velocity to be too high compared to the experiments. We believe that this is a result of the radiative effects, induced by the fast oscillating field and the discreteness of the system as noted above. These effects have been totally neglected in the perturbation treatment, since we here

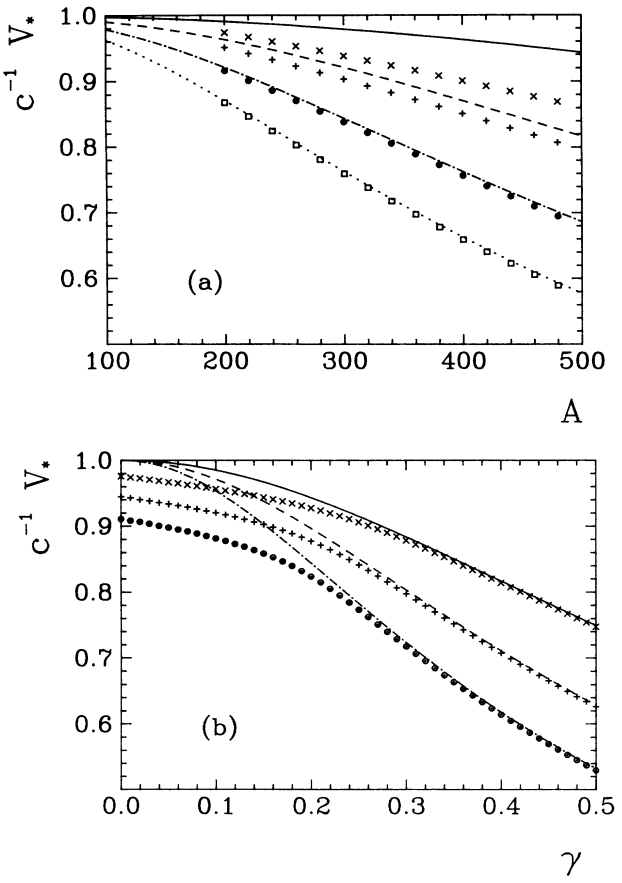

FIG. 3. Comparison between the predicted steady-state velocity [Eq. (19)] (lines) and the results of numerical experiments (markers) made on the system Eq. (30). Parameters are $\Delta x = 0.1$, $L = 100$, and $\omega = 100$. (a) The kink velocity as a function of the driving amplitude A for different values of the dissipation parameter γ. $\gamma = 0.1$: (solid/cross), $\gamma = 0.2$: (dashed/plus), $\gamma = 0.3$: (dash-dotted/circled point), $\gamma = 0.4$: (dotted/square). (b) The kink velocity as a function of the dissipation parameter γ for different values of the driving amplitude A. $A = 250$: (solid/cross), $A = 350$: (dashed/plus), $A = 450$: (dash-dotted/circled point).

have assumed a continuous system with the time-independent *effective* potential. This then leads to too high an estimate of the velocity. For larger values of the damping γ the radiative effects are of course damped more (see Fig. 2), which then leads to a better agreement between the analytical results and the measurements. In Fig. 3 the transition from dissipative losses to radiative losses is visible. As the dissipation parameter γ is decreased, we observe an increasing discrepancy between the perturbation result and the results of the numerical experiments. Further, we find that the measured velocities are in all cases smaller than the predicted, indicating that some losses in the π kink dynamics are not considered in the perturbation treatment. This trend is also verified by the observation of the behavior of the velocity as a function of the driving field amplitude A for $\gamma = 0$ [Fig. 3(b)]. Here, we find, as is intuitively expected, that an increasing field amplitude gives rise to increasing radiative losses, causing a decreasing velocity of the kink. In the numerical experiments, resulting in Fig. 3, we have initiated the π kink in the center of the system with a velocity of $V_* c^{-1} = 0.5$. This initial velocity was necessary to avoid spatially trapped kinks in the cases of relatively small γ and relatively large A values. The trapping of the kinks may be a consequence of the radiative effects, but more likely it is caused by the very high potential hill (see Fig. 1) separating two neighboring pendulums in the $\Phi = 0$ and the $\Phi = \pi$ wells, respectively. So we believe this to be an effect of the discreteness of the system.

In Fig. 4 we show the more complicated situation of the collision between two π kinks, moving in opposite directions. The two kinks have been initiated at $x = 25$ and $x = 75$, respectively. Here we show only the center section of the system ($x = 45$ to $x = 55$) as the collision takes place. Figs. 4(a) and 4(b) show the same event, but for two different values of dissipation, $\gamma = 0.1$ and $\gamma = 0.2$, respectively. In both cases, we observe that the colliding π kinks eventually form a bound state as a 2π kink as may also be predicted by the continuous effective potential model Eq. (20). Another type of collision between kinks is shown in Fig. 5, where the collision between π kink and an anti-π kink is shown for the two dissipation parameters used in Fig. 4. This type of collision

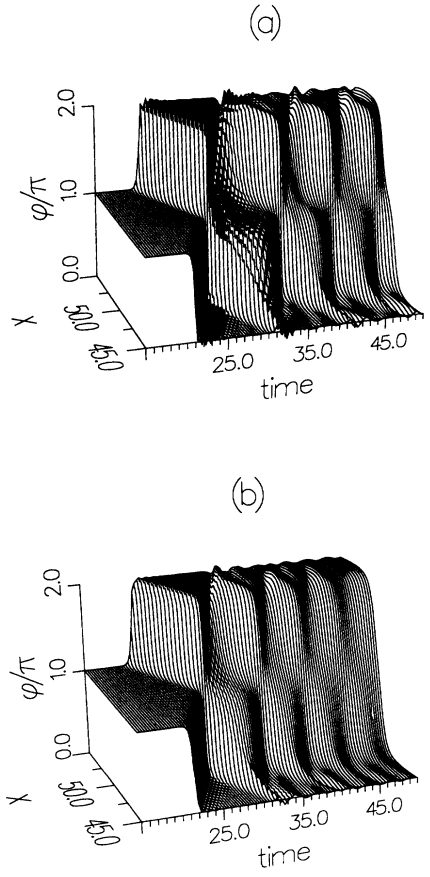

FIG. 4. Collision between two π kinks. Parameters are as in Fig. 2. (a) $\gamma = 0.1$, (b) $\gamma = 0.2$.

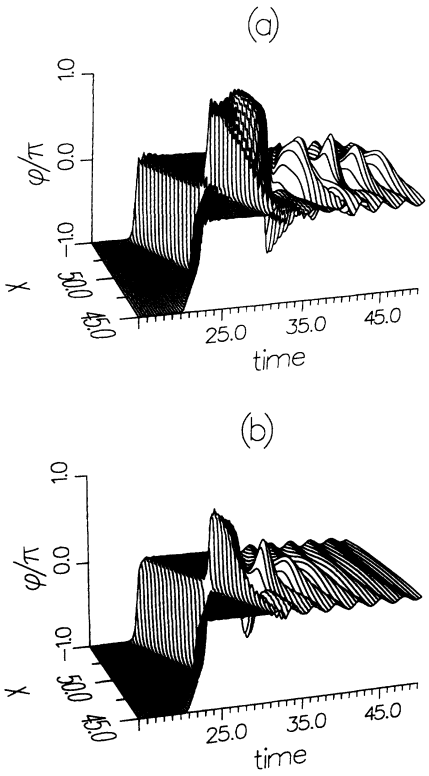

FIG. 5. Collision between a π kink and an anti-π kink. Parameters are as in Fig. 2(a) $\gamma=0.1$, (b) $\gamma=0.2$.

is very similar to the collision of two 2π kinks of opposite polarities observed in the standard continuous SG system. The two kinks are, due to dissipation (and radiative effects), trapped in an oscillating bound state, which in the SG system can be denoted by the breather solution. As seen from Fig. 5, this oscillating mode will eventually decay away. We note here that the direction of motion for a π kink is always so that $|\phi|=\pi$ states are converted to $\phi=0$ states. This implies that if two π kinks move towards each other and collide, so will a pair of a π kink and an anti-π kink. Similarly, we can note that if two π kinks travel away from each other, so will the pair of kink and antikink. This is unlike the behavior of the 2π kinks in the standard SG model, where two kinks of equal polarity always will attract each other.

IV. CONCLUSIONS

In conclusion, we have analyzed the dynamics of the sine-Gordon model in the presence of a high-frequency parametric force. Using the analytical approach based on the averaged equation of motion for the slowly varying field component, we have demonstrated that the effective potential energy of the system allows propagation of localized π kinks if the amplitude of the parametric force exceeds a certain critical value. In the presence of dissipative losses, the π kink propagates at a fixed velocity which is a function of the driving parametric force amplitude and dissipation parameter.

We have also analyzed envelope solitons in the discrete carrier limit, which may be stable at the level $\phi=\pi$ supported by the parametric force.

By means of direct numerical simulations we have showed that the stable propagation of the π kinks can in fact be observed, provided that the force amplitude is large enough. The results of our analytical approach and numerical simulations are in good agreement.

*On leave from Institute for Low Temperature Physics and Engineering, 47 Lenin Avenue, 310164 Kharkov, U.S.S.R.

[1]Yu. S. Kivshar and B. A. Molomed, Rev. Mod. Phys. **61**, 763 (1989).

[2]A. R. Bishop, K. Fesser, P. S. Lomdahl, and S. E. Trullinger, Physica D **7**, 259 (1983).

[3]A. Mazor and A. R. Bishop, Physica D **27**, 269 (1987).

[4]N. Grønbech-Jensen, Yu. S. Kivshar, and M. R. Samuelsen, Phys. Rev. B **43**, 5698 (1991).

[5]C. Vanneste, A. Gilbert, P. Sibillot, and D. B. Ostrowsky, J. Low. Temp. Phys. **45**, 517 (1981).

[6]G. Cicogna and L. Fronzoni, Phys. Rev. A **42**, 1901 (1990).

[7]L. D. Landau and E. M. Lifshitz, *Mechanics*, 3rd ed. (Pergamon, New York, 1976).

[8]See, e.g., Tadashi Uchiyama, Phys. Rev. D **14**, 3520 (1976); C. A. Condat, R. A. Guyer, and M. D. Miller, Phys. Rev. B **27**, 474 (1983); M. Salerno and M. R. Samuelsen, Phys. Lett. A **128**, 424 (1988).

[9]A. M. Kosevich and Yu. S. Kivshar, Fiz. Nizk. Temp. **8**, 1270 (1982) [Sov. J. Low Temp. Phys. **8**, 644 (1982)].

[10]M. Remoissenet, Phys. Rev. B **33**, 2386 (1986).

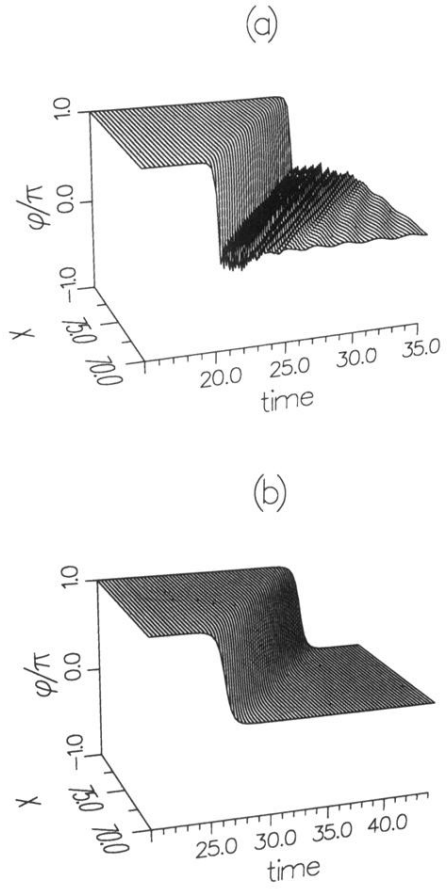

FIG. 2. Steady-state motion of a π kink. Parameters are $\Delta x = 0.1$, $L = 100$, $A = 250$, and $\omega = 100$. (a) $\gamma = 0$. (b) $\gamma = 0.4$.

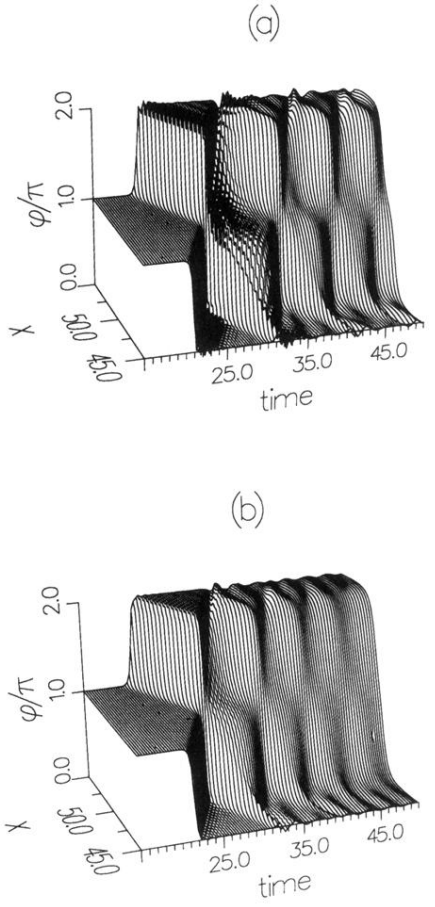

FIG. 4. Collision between two π kinks. Parameters are as in Fig. 2. (a) $\gamma=0.1$, (b) $\gamma=0.2$.

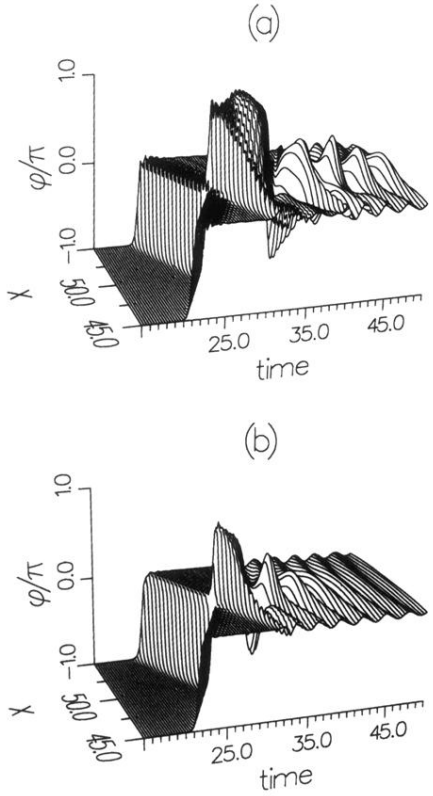

FIG. 5. Collision between a π kink and an anti-π kink. Parameters are as in Fig. 2(a) $\gamma = 0.1$, (b) $\gamma = 0.2$.